RESEARCH ACTIVITIES VI
Department of Vacuum UV Photoscience

VI-A Electronic Structure and Decay Mechanism of Inner-Shell Excited Molecules and Clusters

In this project, we have two major subjects: (a) resonant photoelectron spectroscopy and (b) resonant inelastic soft X-ray emission spectroscopy following inner-shell excitations of simple molecules and clusters. We have found some spin-forbidden ionized and excited states in (a) and (b). In the spectral assignments, angle(symmetry)-resolved photoion yield techniques and R-matrix/MQDT theoretical approaches are essential.

VI-A-1 Rydberg-Valence Mixing in Core Excitations of C_2H_2. Angle-Resolved Photoion Yield Spectroscopic Study

MASUDA, Suomi[1]; GEJO, Tatsuo[2]; HIYAMA, Miyabi; KOSUGI, Nobuhiro
([1]GUAS; [2]Univ. Hyogo)

[*J. Electron Spectrosc.* in press]

High-resolution angle-resolved ion-yield spectra (ARPIS) are reported for the C1s → Rydberg excitations of acetylene. Vibronic coupling features are found in the energy regions of $3s\sigma_g$ and $3\sigma_u$* excitation, $3p\sigma_u$ excitation, and near threshold. Figure 1 shows ARPIS of C_2H_2 measured at the C1s → 3s and 3p Rydberg excitation region. To select the fragmentation channels, we varied the retarding potentials for ion detectors. The contributions of the $3s\sigma_g$ Rydberg state and $3\sigma_u$* valence state were successfully resolved. Consequently, the feature observed in the perpendicular direction is assigned to the C1s → $3\sigma_u$* valence state coupled with the C1s → π* state *via cis* bending vibrational mode.

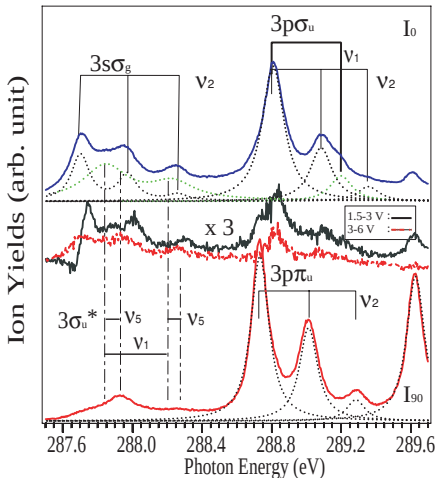

Figure 1. ARPIS of C_2H_2 measured at the C1s → 3s and 3p Rydberg region. Spectra shown on the upper side and lower side correspond to the ion yields measured in the parallel and perpendicular directions, respectively. Spectra shown on the middle are the subtraction spectra measured in the parallel direction with different retarding potentials. : for example, "1.5–3.0 V" means [1.5 V spectra]–[3.0 V spectra].

VI-A-2 Ab Initio R-Matrix/Multi-Channel Quantum Defect Theory Approach to Study Molecular Core Excitation and Ionization: GSCF4R

HIYAMA, Miyabi; KOSUGI, Nobuhiro

[*J. Theor. Comput. Chem.* in press]

Ab initio R-matrix/MQDT approach, which is a combination of *ab initio* R-matrix techniques and the multi channel quantum defect theory (MQDT), has recently been developed by one of the present authors (MH) and Child,[1)] to successfully obtain the potential energy curves of Rydberg states converging to not only the lowest but also the higher ionized states. This approach is also applied to analyze changes in the MQDT scattering matrix arising from the valence state interaction with Rydberg channels.[1)] In the calculations for valence and Rydberg states, the UK molecular R-matrix package developed by Morgan, Tennyson, and Gillan[2)] has been used.

At IMS we extensively study core excitation and ionization of molecules theoretically as well as experimentally. For this purpose we have developed an original *ab initio* polyatomic R-matrix/MQDT code using Gaussian type basis functions (GTFs) for the bound and continuum states with a core hole. Our new program package named GSCF4R is an extension from the conventional *ab initio* SCF-CI (self-consistent field, configuration interaction) package, GSCF3 by one of the present authors (NK), which can be used for both valence and core excitation.[3)]

References

1) M. Hiyama and M. S. Child, *J. Phys. B* **35**, 1337 (2002) ; **36**, 4547 (2003) .
2) L. A. Morgan, J. Tennyson and C. J. Gillan, *Comput. Phys. Commun.* **114**, 120 (1998).
3) N. Kosugi and H. Kuroda, *Chem. Phys. Lett.* **74**, 490 (1980); *Theor. Chim. Acta* **72**, 149 (1987).

VI-A-3 Ab Initio R-Matrix/Multi-Channel Quantum Defect Theory Applied to Molecular Core Excitation and Ionization

HIYAMA, Miyabi; KOSUGI, Nobuhiro

[*J. Electron Spectrosc.* in press]

Very recently we have completed an original ab initio polyatomic R-matrix/MQDT program package, GSCF4R[1)] based on Gaussian type basis functions (GTFs) for the bound and continuum states, to extensively study molecular excitation and ionization in the X-ray region as well as in the VUV region. Calculated results for core excitation and ionization of NO show that the R-matrix/MQDT method is indispensable to describe the core-to-Rydberg states with the higher quantum number and the continuum states which cannot be described by using GTFs in the outer region of an appropriate boundary. In the inner region the close-coupling approximation augmented with the correlation term in GSCF4R is proved to be powerful to obtain the potential energies of valence and Rydberg-valence mixed states and the interchannel couplings between several core-ionized states.

Reference

1) M. Hiyama and N. Kosugi, *J. Theor. Comput. Chem.* in press.

VI-A-4 Valence in the Rydberg/Continuum Region in Molecular Inner-Shell Spectroscopy

KOSUGI, Nobuhiro

[*J. Electron Spectrosc.* in press]

Using schematic potential energy curves and molecular orbitals, we have discussed where the 1s → σ* excited state is located in the 1s excitation of N_2, O_2, CH_3F, and C_2H_2, and how we know evidence for the 1s → σ* excited state in photoabsorption spectra of CH_4, CO_2, and N_2O. In the former molecules, the σ* state is identified in the Franck-Condon region from the ground state; in the latter molecules, the σ* state is not clearly identified but its evidence is observed through the Rydberg-valence mixing in the Franck-Condon region. In N_2, the σ* state is located above the ionization threshold and is autoionizing. In O_2, the σ* state is mainly mixed with the 3pσ* Rydberg state converging to the $^4\Sigma$ ionized state. In CH_3F, the σ* state is observed below the 3s Rydberg state. In C_2H_2, the σ* state and the 3s Rydberg state are observed in the same energy region and the σ* state has an effect of the conical intersection with the lowest π* state, where the σ* state is lower than the π* state for a longer HCC–H distance. On the other hand, in CH_4, the Jahn-Teller distortion of the 3p Rydberg transition induces contribution from the σ* state. In the 1s excitations from the terminal atoms in CO_2 and N_2O, some lower s-type Rydberg states get intensities from the σ* state. In the 1s excitations from the central atoms, the σ* state is a dark state (not exactly in N_2O). In the C1s excitation of CO_2, the 3s Rydberg states are vibronically enhanced through mixing with the π* state.

VI-A-5 Spin-Orbit and Exchange Interactions in Molecular Inner-Shell Spectroscopy

KOSUGI, Nobuhiro

[*J. Electron Spectrosc.* **137-140**, 335 (2004)]

In recent high-resolution and sophisticated soft X-ray molecular spectroscopies, small exchange interaction (EX) involving the core electron has been revealed. Interatomic core-core EX is generally small; therefore, it is considered that even the core electron described as $1s\sigma_g$ and $1s\sigma_u$ in homonuclear systems is localized on an atom. However, small but appreciable interatomic core-valence EX in N_2 and C_2H_2 results in observable *g-u* splittings in the core ionization, which are experimentally evaluated from extrapolation of the $1s\sigma_g^{local} \rightarrow np\sigma_u$, $np\pi_u$ and $1s\sigma_u^{local} \rightarrow ns d\sigma_g$, $nd\pi_g$ Rydberg series. Due to intermolecular Rydberg-valence EX, blue shifts in low-lying core-to-Rydberg excitations in N_2 and Ar are experimentally identified from gas phase to surface, from surface to bulk, and from large to small cage size of rare gas matrixes. EX involving the 2p core electron is anisotropic, depending on the relation between the 2p orbital direction and molecular structure. In some sulfur containing molecules, it is experimentally revealed that the S2p and excited electrons have EX compatible to the 2p spin-orbit interaction (SO) for parallel 2pπ → π* transitions and EX smaller than SO for perpendicular 2pσ → π* transitions. In other words, the *jj* coupling scheme is not applicable to the parallel transitions. Furthermore, it is revealed that, in resonant photoelectron and soft X-ray emissions on the S2p excitation of CS_2 and SF_6, spin-forbidden shake-up valence ionizations with quartet spin couplings and spin-forbidden valence excitations with triplet spin couplings are observable *via* triplet components mixed in intermediate core-excited states.

VI-B Soft X-Ray Photoelectron-Photoabsorption Spectroscopy and Electronic Structure of Molecular Solids and Clusters

This project has been carried out in collaboration with Würzburg University and RIKEN. We have two subprojects: (a) molecules and radicals in condensed phase and in rare gas matrix, and (b) ionic fragmentations of atomic and molecular clusters following the inner-shell resonance excitation. In (a), we have measured excitation spectra of some matrix phases and of some bases in DNA duplexes at the bending-magnet beamline BL4B of the

UVSOR facility. In (b), we have developed a new cluster source for photoelectron measurements on a newly constructed undulator beamline BL3U.

VI-B-1 Temperature Dependence of the Bulk Ar $2p_{3/2}$-4s Excited State of Argon Solid

HATSUI, Takaki; SETOYAMA, Hiroyuki; KOSUGI, Nobuhiro

[*J. Electron Spectrosc.* in press]

Core excitons of rare gas solid have been studied extensively in order to elucidate their character. In the present study, the Ar $2p_{3/2}$-4s excited state for bulk argon solid has been investigated at 8 and 16 K (Figure 1). Careful energy calibration of the monochromater has demonstrated that the peak position at 16 K shows a red shift of 4.2 ± 0.9 meV compared with that at 8 K. The increase of the temperature from 8 to 16 K results in the elongation of the lattice constant of the argon solid from 5.290 to 5.294 Å. The larger lattice constant is expected to cause a blue shift in ionization threshold caused by the weaker stabilization through polarization interaction (PL) of the surrounding atoms/molecules, and a red shift by the weaker exchange interaction (EX) between the excited electron and the electrons of neighboring atoms/molecules. In order to quantitatively examine the observed temperature dependence, *ab initio* theoretical calculations has been carried out for Ar_{19} cluster. The calculations predict the red shift to be 2.7 meV as a sum of the blue shift of 1.1 meV through PL and the red shift of 3.8 meV through EX. The agreement of the theory with the experiment implies the reliability of the calculations. The mean radius of the 4s excited orbital is predicted to be 5.80 Å.

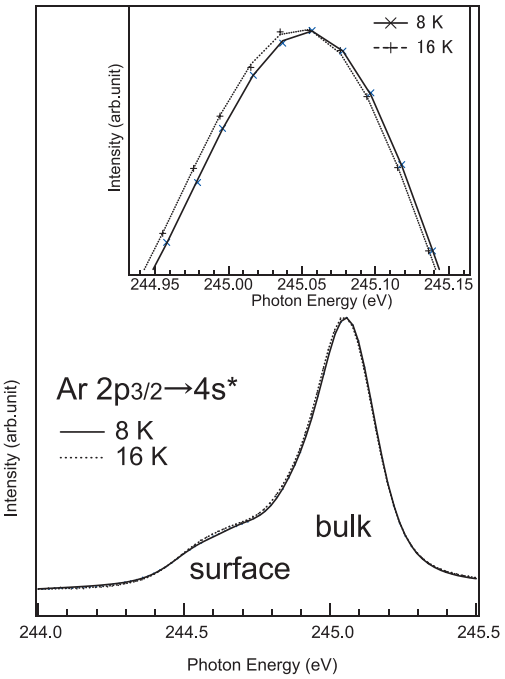

Figure 1. Photoabsorption spectra for argon solid around the Ar $2p_{3/2}$-4s bands at 8 and 16 K. Enlarged spectra around the peak of the bulk Ar $2p_{3/2}$-4s band are shown in inset.

VI-B-2 Sulfur 2p Excited States of OCS in Rare Gas Matrices

SETOYAMA, Hiroyuki; HATSUI, Takaki; KOSUGI, Nobuhiro

[*J. Electron Spectrosc.* in press]

Sulfur 2p x-ray absorption spectra have been measured for OCS solid and for the mixture of OCS and Ar, Kr or Xe in order to study effects of surrounding molecules on the S 2p excited states of OCS. Figure 1 shows S 2p photoabsorption spectra of OCS solid and Xe matrices for different concentration ratios, OCS:Xe = 1:0, 1:1, and 1:7/3. Bands 1 and 2 are assigned to the S $2p_{3/2}$- and S $2p_{1/2}$-4π* core-to-valence transitions, respectively. Bands 3, 4, 5 and 6 are assigned to the $2p_{3/2}$-4s, $2p_{1/2}$-4s, $2p_{3/2}$-"d", and $2p_{1/2}$-"d" transitions with Rydberg character, respectively. The core-to-valence excited states (bands 1 and 2) do not change their positions upon the mixing, whereas the excited states originating from Rydberg 4s and "d" states show energy shifts. The observed dependence of the shifts on the mixing concentration and on the rare gas element were explained in terms of the polarization stabilization of the ionization threshold and the exchange repulsion of the excited electron by the electrons of the neighboring atoms/molecules. At the same mixing ratio, the polarization stabilization was found to be independent of the rare gas element.

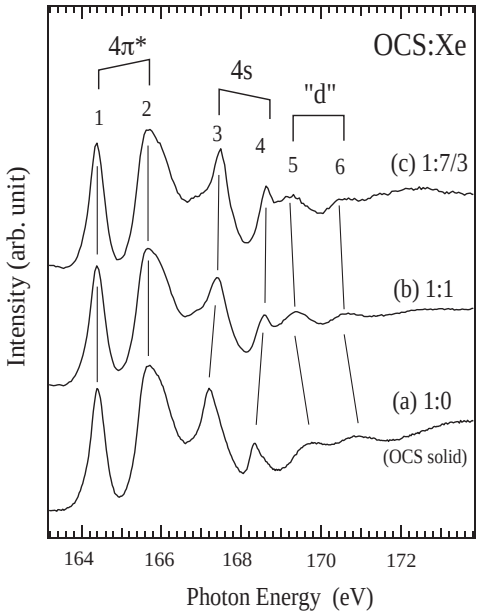

Figure 1. Soft X-ray absorption spectra for OCS and OCS/Xe matrices with different ratios, 1:1 and 1:7/3.

VI-B-3 Cluster Size Effects in Core Excitons of 1s-Excited Nitrogen

FLESCH, Roman[1]; KOSUGI, Nobuhiro;

BRADEANU, Ioana[1]; NEVILLE, John[2]; RÜHL, Eckart[1]
([1]Würzburg Univ.; [2]Univ. New Brunswick)

[*J. Chem. Phys.* **121**, 8343 (2004)]

Cluster size effects in core excitons below the N 1s ionization energy of nitrogen clusters are reported in the energy regime 405–410 eV. These results are compared to the molecular Rydberg states as well as the corresponding bulk excitons of condensed nitrogen. The experimental results are assigned using *ab initio* calculations. It is found that the lowest excitons (N 1s → 3sσ and N 1s → 3pπ) are blueshifted relative to the molecular Rydberg transitions, whereas others (N 1s → 3dπ and N 1s → 4pπ) show a redshift. Results from *ab initio* calculations on $(N_2)_{13}$ clearly indicate that the molecular orientation within a cluster is critical to the spectral shift, where bulk sites as well as inner- and outer-surface sites are characterized by different inner-shell absorption energies. These results are compared to the experimental spectra as well as previous work on site-selectively excited atomic van der Waals clusters, providing an improved spectral assignment of core exciton states in weakly bound molecular clusters and the corresponding condensed phase.

VI-B-4 Metal-to-Ligand Charge Transfer in Polarized Metal L-Edge X-Ray Absorption of Ni and Cu Complexes

HATSUI, Takaki; KOSUGI, Nobuhiro

[*J. Electron Spectrosc.* **136**, 67 (2004)]

Metal L-edge X-ray absorption spectra for Ni and Cu complexes are discussed by investigating their linear polarization dependence. The origin of the characteristic bands is revealed to be one-electron transitions to ligand-centered molecular orbitals carrying metal-to-ligand charge transfer (MLCT). We have shown that the strong bands B and C in $K_2[Ni(CN)_4]\cdot H_2O$ and Ni $(Hdmg)_2$ are definitely assigned to the MLCT transitions by examining the linear polarization dependence and by carrying out *ab initio* molecular orbital calculations. The MLCT transitions are also found in metal $L_{2,3}$-edge X-ray absorption spectra of $[(n\text{-}C_4H_9)_4N]_2[Ni(mnt)_2]$, $(Me_2\text{-}DCNQI)_2Cu$, $K_3Cu(CN)_4$, and $[(C_2H_5)_4N][Ni(mnt)_2]$. It is shown that the intensity of the MLCT transitions is directly correlated to the strength of the back-donation, in which the excited orbital is involved. The linear polarization dependence is also useful to reveal the symmetry of the holes in doped systems and to characterize the Ni–Ni chemical bonding.

VI-B-5 Electronic Structure of Bases in DNA Duplexes Characterized by Resonant Photoemission Spectroscopy near the Fermi Level

KATO, Hiroyuki S.[1]; FURUKAWA, Masashi[1]; KAWAI, Maki[1,2]; TANIGUCHI, Masaki[3]; KAWAI, Tomoji[3]; HATSUI, Takaki; KOSUGI, Nobuhiro
([1]RIKEN; [2]Univ. Tokyo; [3]Osaka Univ.)

[*Phys. Rev. Lett.* **93**, 086403 (2004)]

The electronic structure of bases in DNA duplexes was investigated by resonant photoemission spectroscopy near the Fermi level, in order to specify charge migration mechanisms. Figure 1(A) shows an N K-edge XA spectrum of poly(dG)·poly(dC) and DNA. In the XA spectrum, two 1s → π* resonant peaks at 399.7 eV and 401.9 eV and a broad 1s → σ* resonant peak at 407 eV were observed. This spectrum is in good agreement with the previously reported XA spectra of poly(dG)·poly(dC) DNA,[1)] in which the first (energetically lower) and the second (higher) 1s → π* resonant peaks have been assigned to resonance at imine (–N) and amine (–NH–) site orbitals, respectively. The off-and-on-RPE spectra near the Fermi level of poly(dG)·poly(dC) DNA are shown in Figure 1(B) as a function of kinetic energy. The Auger signals can be extracted from the on-RPE spectra by subtracting the off-RPE spectra, as indicated by the dotted lines. A kinetic energy shift of N-KLL Auger electrons and an intensity enhancement of valence electrons on the resonant photoemission spectra are clearly observed. Similar behaviors are also found for poly(dA)·poly(dT) DNA. These directly show the localized unoccupied states of the bases. We conclude that the charge hopping model is suitable for electric conduction in DNA duplexes rather than the charge transfer model *via* delocalized states when electrons pass through the π* states of DNA bases.

Reference

1) S. M. Kirtley *et al.*, *Biochim. Biophys. Acta* **1132**, 249 (1992).

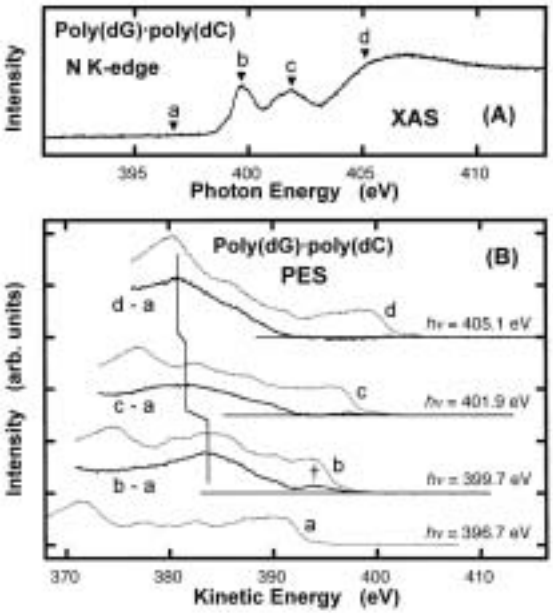

Figure 1. N K-edge XA spectrum of poly(dG)·poly(dC) DNA (A), and its off- and on-RPE spectra as functions of kinetic energy (B). Excitation enegies are shown as arrows a–d in Figure 1(A). The differential spectra based on the off-RPE spectrum in binding energy show resonant Auger signals.

VI-C Ultrafast Dynamics of Molecules in Intense Laser Fields

The interaction between molecules and an intense laser field (10^{12}–10^{18} W/cm^2), whose electric field component comparable with the intramolecular Coulombic field, has been an attractive target of research to elucidate fundamental physical properties underlying in the unique features that do not appear in the weak interaction regime. In the present study, the characteristic dynamics occurring in intense laser fields, such as structural deformation and multiple breaking of chemical bonds, is studied by a newly developed experimental method, called *coincidence momentum imaging*, which allows us to determine the momentum vectors of all the fragment ions ejected from a single parent molecule in an intense laser field. Based on the correlation among the fragment momentum vectors, the evolution of nuclear motion on the light dressed potential energy surfaces and the hydrogen migration process have been clarified. A new coincidence momentum imaging system is constructed to detect the ions and electrons produced from a molecule placed in an intense laser field.

VI-C-1 Nuclear Dynamics on the Light-Dressed Potential Energy Surface of CS_2 by Coincidence Momentum Imaging

HISHIKAWA, Akiyoshi; HASEGAWA, Hirokazu[1]; YAMANOUCHI, Kaoru[1]
([1]Univ. Tokyo)

[*Chem. Phys. Lett.* **388**, 1–6 (2004)]

The non-sequential three-body Coulomb explosion, $CS_2^{3+} \rightarrow S^+ + C^+ + S^+$, in an intense laser field (0.2 PW/cm^2, 60 fs) is studied by the coincidence momentum imaging of the fragment ions. The observed angle distribution of the momentum vectors of the two S^+ ions, $\boldsymbol{p}_1(S^+)$ and $\boldsymbol{p}_2(S^+)$, exhibited a peak at the small angle $\theta_{12} \sim 140°$, showing that the nuclear motion is induced along the bending coordinate to a large extent prior to the explosion. On the other hand, the difference between their absolute values, $\Delta p_{12} = |\boldsymbol{p}_1(S^+)| - |\boldsymbol{p}_2(S^+)|$, has a sharp distribution peaked at $\Delta p_{12} = 0$, suggesting that the symmetric stretching motion dominates over the anti-symmetric stretching motion in the laser field. Based on the energy dependence of the momentum vector correlation, the characteristic nuclear dynamics of CS_2 on the light-dressed potential energy surfaces in the intense laser field is discussed.

VI-C-2 Hydrogen Migration in Acetonitrile in Intense Laser Fields Studied by Coincidence Momentum Imaging

HISHIKAWA, Akiyoshi; HASEGAWA, Hirokazu[1]; YAMANOUCHI, Kaoru[1]
([1]Univ. Tokyo)

[*Phys. Scr.* **T108**, 108–111 (2004)]

The two-body Coulomb explosion of acetonitrile, $CH_3CN^{2+} \rightarrow CH_{3-n}^+ + H_nCN^+$ (n = 0–2), in intense laser fields (0.15 PW/cm^2, 70 fs) is studied by the coincidence momentum imaging technique. It is found that the fragment ions for n = 0 are ejected mostly to the direction of the laser polarization vector with $\langle\cos^2\theta\rangle$ = 0.68, where θ is the angle between the fragment recoil direction and the laser polarization vector, while the angle distribution becomes more isotropic as n increases, *i.e.*, $\langle\cos^2\theta\rangle$ = 0.49 for n = 1 and $\langle\cos^2\theta\rangle$ = 0.37 for n = 2. From this characteristic correlation between the anisotropy in the fragment ejection and the hydrogen migration, the Coulomb explosion dynamics competing with the hydrogen atom transfer from the methyl group to the nitrile group is investigated.

VI-C-3 Hydrogen Migration in Acetonitrile in Intense Laser Fields in Competition with Two-Body Coulomb Explosion

HISHIKAWA, Akiyoshi; HASEGAWA, Hirokazu[1]; YAMANOUCHI, Kaoru[1]
([1]Univ. Tokyo)

[*J. Electron. Spectrosc. Relat. Phenom.* **141**, 195–200 (2004)]

Two-body Coulomb explosion processes of acetonitrile (CH_3CN) and deuterated acetonitrile (CD_3CN), $CH_3CN^{2+} \rightarrow CH_{3-n}^+ + H_nCN^+$ and $CD_3CN^{2+} \rightarrow CD_{3-n}^+ + D_nCN^+$ (n = 0, 1, 2), in an intense laser field (0.15 PW/cm^2, 70 fs) are investigated by the coincidence momentum imaging method. The comparable yields derived for the three pathways (n = 0, 1, 2) shows that the hydrogen atom migration proceeds in competition with the Coulomb explosion. The angular distributions of the fragment ions for n = 0 exhibits a sharp peak along the laser polarization direction, while the angular distribution becomes more isotropic as n increases. Based on a least-squares analysis of the fragment anisotropy, the dissociation lifetimes of the doubly charged acetonitrile were determined, from which the time scale of the hydrogen migration as well as the deformation of the C–C–N skeleton prior to the explosion were discussed.

VI-C-4 Design and Development of an Ion-Electron Coincidence Momentum Imaging System

HISHIKAWA, Akiyoshi; TAKAHASHI, Eiji J.

A new coincidence momentum imaging system has been developed to study the behavior of molecules exposed to an intense laser field ($\sim 10^{15}$ W/cm^2) based on the momentum vectors of fragment ions and electrons ejected from a single parent molecule. The electrons and ions are guided by electrodes in the velocity mapping configuration and detected by a pair of position sensitive detectors with delay line anodes,

which are placed face by face in an ultrahigh vacuum chamber with a base pressure < 10^{-8} Pa. The performance of the electron detection has been studied with Xe and CS_2 in an intense laser field (~ 10^{13} W/cm^2, 35 fs, 800 nm). The concentric ring patterns visible in the electron image (Figure 1), separated by the photon energy (~ 1.5 eV) in the energy scale, represent the above-threshold ionization (ATI) process.

Figure 1. Electron image obtained for CS_2 in an intense laser field (1.5 × 10^{13} W/cm^2, 35 fs, 800 nm). In order to to emphasize weak features, a logarithmic intensity scale is adopted. The concentric ring patterns represent the ATI process.

VI-D Synchrotron Radiation Stimulated Surface Reaction and Nanoscience

Synchrotron radiation (SR) stimulated process (etching, CVD) has excellent characteristics of unique material selectivity, low damage, low contamination, high spatial resolution, and high precision etc. In this project, nano-level controlled structures are created by using synchrotron radiation stimulated process, and the reaction mechanisms are investigated by using STM and AFM. Concerning the SR etching, we are considering to apply this technique to the microfabrication of integrated protein transistor circuits.

VI-D-1 Construction of Undulator Beamline for STM Observations of Surface Reaction Stimulated by Synchrotron Irradiation

NONOGAKI, Youichi; URISU, Tsuneo

[*J. Electron Spectrosc. Relat. Phenom.* submitted]

To investigate excitation energy dependence of SR-stimulated reactions, we have designed and constructed an undulator beamline equipped with an UHV-STM system at the UVSOR facility. Since 1st harmonic emission from the undulator is changed from 50 eV to 120 eV, it is possible that the emission is tuned to Si 2p (~100 eV) core-level. The undulator emission is focused by two cylindrical mirrors. The spot size is 1.0 mm × 0.4 mm and photon flux density is estimated to 10^{18} $cm^{-2}sec^{-1}$ on a sample surface in the UHV-STM chamber set at the end station.

Although ESD of H-Si(111) surfaces have been studied extensively, there is no report of photon-stimulated reaction on the H-Si(111) surfaces observed by STM. We have successfully observed morphological changes of H-Si(111) after undulator irradiation by STM. Figure 1(a) shows an STM image of a H-Si(111) prepared by 1000L H-exposure to a clean Si(111)-7×7 surface at 400 °C. A 7×7 rest-atom monohydride surface appeared with adatom islands (A) and small protrusions (B). This surface was exposed to undulator irradiation (~ 100 eV) at an irradiation dose of 4900 mAsec. Figure 1(b) shows an STM image of the surface after irradiation. It is found that density of the small protrusions drastically increased on the 7×7 rest-atom monohydride surface. Creation of the small protrusions would be related to H-desorption stimulated by undulator irradiation.

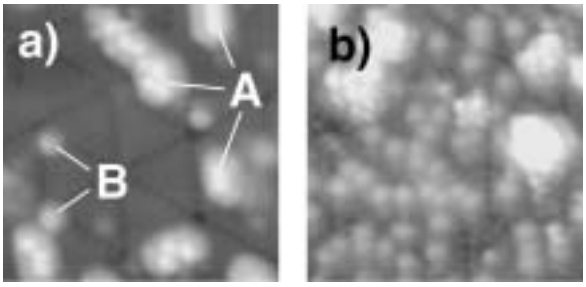

Figure 1. 11 nm × 11 nm STM images of a) H-Si(111) surface and b) surface after undulator irradiation.

VI-D-2 Shrinking of Spin-On-Glass Films Induced by Synchrotron Radiation and Its Application to Three-Dimensional Microfabrications

RAHMAN, Md. Mashiur; TERO, Ryugo; URISU, Tsuneo

[*Jpn. J. Appl. Phys.* **43**, 4591–4594 (2004)]

Photoinduced etching of siloxane-type spin-on-glass (SOG) by synchrotron radiation (SR) using a SF_6/O_2 etching gas and a Co contact mask has been investigated. The SOG film was etched by direct SR irradiation similarly to the case of thermally oxidized SiO_2. We found that the indirect exposure to SR caused shrinkage of SOG under the Co mask. The shrinkage depth of SOG was attenuated by the thickness of the Co mask, but not eliminated even by a Co mask 350 nm thick, due to the highenergy photons (230 eV) being transmitted through the mask. The shrinkage phenomenon was successfully applied in the fabrication of a three-dimensional structure of the SOG thin film on Si(100). Atomic force microscopy observations showed that the surfaces were very smooth both on the completely etched Si area and on the shrunken SOG area. We investigated the mechanism of the shrinkage of SOG by Fourier-transform infrared spectroscopy.

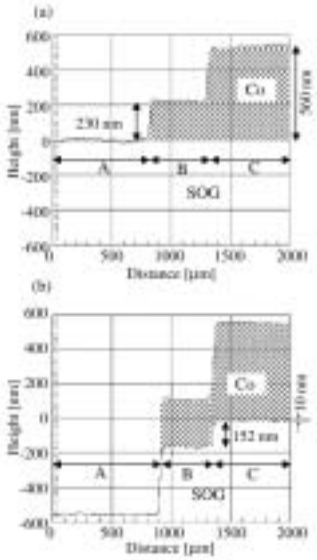

Figure 1. Step profiles of the Co/SOG/Si surface (a) before and (b) after SR etching. The step profile of SOG/Si after removal of the Co layer is superimposed in (b).

VI-E Noble Semiconductor Surface Vibration Spectroscopy

As a new high sensitive and high resolution surface vibration spectroscopy technique, we are developing an infrared reflection absorption spectroscopy using buried metal layer substrate (BML-IRRAS), which have unique characteristics of high resolution and high sensitivity at finger print regions. Several Si surface chemical reactions are investigated using this BML-IRRAS. As a new fabrication technique of BML substrate, we have almost succeeded in developing the wafer bonding technique. It is considered that BML-IRRAS is also extremely useful in the research of bio-material integration on Si substrates.

VI-E-1 Three-Pairs of Doublet Bands Assigned to SiH_2 Scissoring Modes Observed in H_2O-Induced Oxidation of Si(100) Surfaces

WANG, Zhi-Hong; URISU, Tsuneo; NANBU, Shinkoh; MAKI, Jun; GANGAVARAPU, Ranga Rao; AOYAGI, Mutsumi[1]; WATANABE, Hidekazu[1]; OOI, Kenta[2]
([1]Kyushu Univ.; [2]AIST Shikoku)

[*Phys. Rev. B* **69**, 045309 (5 pages) (2004)]

Oxidation of Si(100) surfaces by H_2O has been investigated on $2H+H_2O$/Si(100)-(2×1), H_2O Si(100)-(2×1), as well as H_2O+H/Si(100)-(2×1) systems by infrared reflection absorption spectroscopy using $CoSi_2$ buried metal layer substrates BML-IRRAS. Three pairs of doublet bands assigned to the scissoring modes of adjacent and isolated SiH_2 with zero, one, and two inserted back-bond oxygen atoms, respectively, have been reported. This report also has clearly shown the unique high sensitivity of BML-IRRAS for the perpendicular components in the fingerprint region, compared to the multiple internal reflection and the external transmission arrangements. Oxidation mechanisms have been proposed. In the $2H+H_2O$/Si(100)-(2×1) system, oxygen insertion into the back bond occurs easily. In the H_2O+H/Si(100) system, however, the tunneling effect is important to reach the oxygen inserted state.

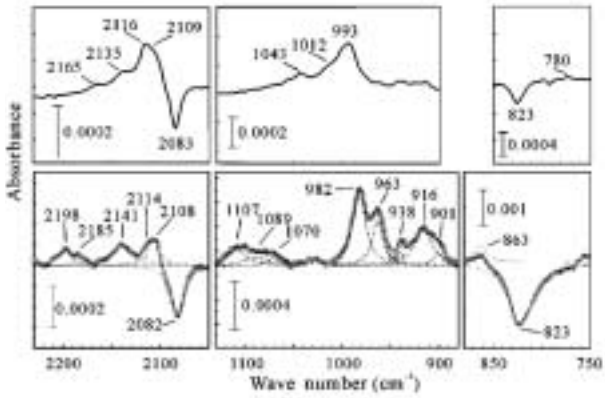

Figure 1. Observed BML-IRRAS spectrum (circles, in the lower panel) of the reaction system $2H+H_2O$(5×l)/Si(100)-(2×1) at T_m = 373 K for D = 1000 l. The curve resolutions assuming a Lorenzian form (solid and dotted lines) are also shown. Compared in the upper part is the reported IR spectrum by ET for the similar reaction system. The three pairs of doublet bands are observed at 982, 963, 938, 926, 916, and 901 cm^{-1}, respectively. The 926-cm^{-1} band, which is not clear in this spectrum, is observed clearly at the lower H doses.

VI-E-2 A Comparative Infrared Study of H_2O Reactivity on Si(100)-(2x1), (2x1)-H, (1x1)-H and (3x1)-H Surfaces

GANGAVARAPU, Ranga Rao; WANG, Zhi-Hong; WATANABE, Hidekazu[1]; AOYAGI, Mutsumi[1]; URISU, Tsuneo
([1]Kyushu Univ.)

[*Surf. Sci.* in press]

The water adsorption on the bare and H-terminated Si(100) surfaces has been studied by the BML-IRRAS technique. It is found that H-terminated surfaces are much less reactive compared to the bare silicon surfaces. The (1×1)-H and (3×1)-H surfaces show similar and less reactivity pattern compared to the (2×1)-H surface. At higher exposures, the water reaction with coupled monohydride species provides an effective channel for oxygen insertion into the back bonds of dihydride species. It is not attributed to the H–Si–Si–H + H_2O → H–Si–Si–OH + H_2, which could give rise to the characteristic Si–H and Si–OH modes, respectively at 2081 and 921 cm^{-1}. A more suitable reaction mechanism involving a metastable species, H–Si–Si–H + H_2O → $H_2Si\cdots HO$–Si–H (metastable) explains well the bending modes of oxygen inserted silicon dihydride species which are observed relatively strongly in the reaction of water with H-terminated Si(100) surfaces.

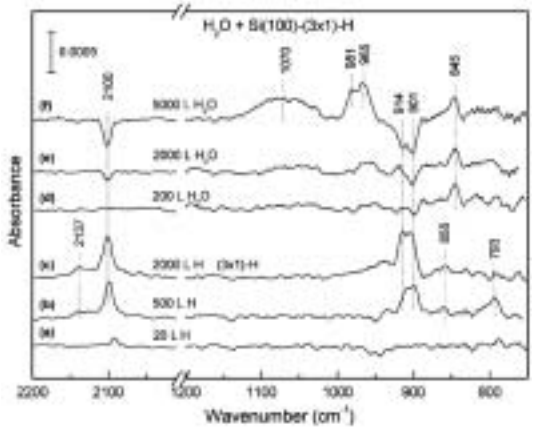

Figure 1. BML-IRRAS spectra of the Si(100)-(3×1)-H surface exposed to (a) 20 L atomic H, (b) 500 L atomic H, (c) 2000 L atomic H, (d) 200 L H_2O, (e) 2000 L H_2O, (f) 5000 L H_2O at 400 K. The spectra (a)–(c) are the ratios of absorption spectra of the H exposed Si(100)-(2×1)-D surfaces to the Si (100)-(2×1)-D surface, and the spectra (d)–(f) are the ratios of the absorption spectra of the water exposed Si(100)-(3×1)-H surfaces to the Si(100)-(3×1)-H surface, recorded at 400 K.

VI-E-3 Theoretical Analysis of the Oxygen Insertion Process in the Oxidation Reactions of H_2O+H/Si(100) and 2H+H_2O/Si(100): a Molecular Orbital Calculation and an Analysis of Tunneling Reaction

WATANABE, Hidekazu[1]; NANBU, Shinkoh; WANG, Zhi-Hong; MAKI, Jun; URISU, Tsuneo; AOYAGI, Mutsumi[1]; OOI, Kenta[2]
([1]Kyushu Univ.; [2]AIST Shikoku)

[*Chem. Phys. Lett.* **383**, 523–527 (2004)]

The reaction paths are analyzed, by an ab initio molecular orbital method, for the surface reaction systems 2H+H_2O/Si(100)-(2×1) and H_2O+H/Si(100)-(2×1), in which SiH_2 species with one or two oxygen atom-inserted back bonds have been observed as stable reaction products. The following results are obtained: The initial energy for the former system is 87.97 kJ/mol higher than the highest transition state energies with the HF/6-31+G* level. In the latter system, the highest transition state is located 175.66 kJ/ mol higher than the initial energy, and tunneling effect plays an important role.

VI-E-4 Fabrication of $CoSi_2$-Buried-Metal-Layer Si Substrates for Infrared Reflection Absorption Spectroscopy by Wafer-Bonding

YAMAMURA, Shusaku; YAMAGUCHI, Shouichi[1]; WATANABE, Satoru[2]; TABE, Michiharu[3]; KASAI, Toshio[4]; NONOGAKI, Youichi; URISU, Tsuneo
([1]DENSO Res. Laboratories; [2]FUJITSU Laboratories Ltd.; [3]Shizuoka Univ.; [4]Saitama Univ.)

[*Jpn. J. Appl. Phys.* **42**, 3942–3945 (2003)]

Infrared reflection absorption spectroscopy (IRRAS) using buried metal layer substrates (BML) is one of the high resolution and high sensitive surface vibration spectroscopy techniques. A unique characteristic is the wide frequency range including the so-called finger print region. The $CoSi_2$ Si(100) BML substrates fabricated by Co ion implantation have been used to date. However, the technique has several problems such as the resultant surface roughness due to the ion implantation damage. To solve these problems, in this work, we have examined the fabrication of BML substrates with atomic-level flat surfaces by the wafer-bonding between a Co deposited Si(100) wafer and a Si on insulator (SOI) wafer. Self-assembled alkyl monolayers (SAMs) of octadecyltrichlorosilane and octenyltrichlorosilane were deposited on the fabricated BML substrate surface. Good BML-IRRAS spectra were observed in the wide frequency range from stretching to bending regions. It was also found that well-ordered SAMs were deposited.

VI-E-5 Design of the Sample Holder System for BML-IRRAS in-Liquid

UNO, Hidetaka; URISU, Tsuneo

We have performed BML-IRRAS in a ultra-high vacuum condition, and investigated hydrogen adsorption on Si clean surfaces. In this report, we present a new project in which the BML-IRRAS is adopted to the bio-material spectroscopy in liquid conditions.

Figure 1 shows a schematic drawing of the sample holder for BML-IRRAS in liquid. The liquid is filled between the BML substrate and the BaF_2 prism. In order to estimate the influence of H_2O to the IR spectrum, we performed calculations with a model in which H_2O was used as a buffer solution. In this model, proteins were substituted by SiC to illustrate the influence of H_2O clearly in the region of Amide I and Amide II bands, because SiC has no spectral features in this region.

The reflectance of the model system was calculated by using the complex refractive indexes of each layer. Figure 2 shows the observed spectrum of the sample with proteins on the BML substrate in a dry condition and the calculated spectrum of the model system described above. Absorption peaks of Amide I and II are clearly seen in the experimental spectrum. In the calculated spectrum, on the other hand, the absorption peak is also seen at 1640 cm^{-1} which is assigned to the absorption peak of H_2O. It will be very difficult to find Amide I and II peaks from the background of H_2O absorption. This problem should be avoided by using D_2O instead of H_2O. The influence of D_2O should be estimated in the near future.

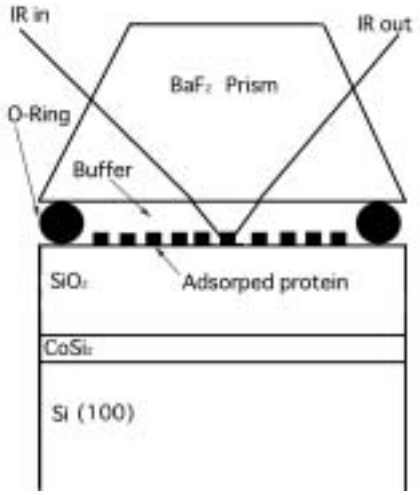

Figure 1. Schematic drawing of the sample holder for BML-IRRAS in liquid.

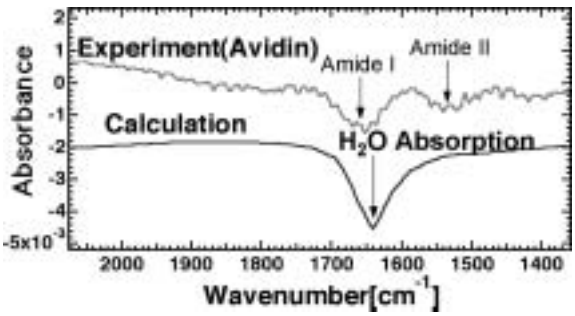

Figure 2. Experimental spectrum of the sample with proteins on the BML substrate in the dry condition and the calculated spectrum of the $BaF_2/H_2O/SiC/SiO_2/Co$ model.

VI-F Integration of Bio-Functional Materials on Silicon

Integration of bio-functional materials such as lipids and proteins are expected to find important applications in biosensors, development of new medicines, and diagnosis of intractable diseases *etc*. In this project, we are investigating the area selective modification of Si surfaces by depositing the self-assembled alkyl monolayers, and the integration of lipid bilayers supporting channel proteins keeping their bio-activities. Our specialinterests are developing "protein transistors" and co-integrating them together with the Si MOS FETs on the same Si chip.

VI-F-1 Deposition of Phospholipid Layers on SiO_2 Surface Modified by Alkyl-SAM Islands

TERO, Ryugo; LI, Yanjun; YAMAZAKI, Masahito[1]; URISU, Tsuneo
([1]Shizuoka Univ.)

[*Appl. Surf. Sci.* in press]

Formation of the supported planar bilayer of dipalmitoylphosphatidylcholine (DPPC) on SiO_2 surfaces modified with the selfassembled monolayer (SAM) of octadecyltrichlorosilane (OTS) has been investigated by atomic force microscopy (AFM). DPPC was deposited by the fusion of vesicles on SiO_2 surfaces with OTS-SAM islands of different sizes and densities. The DPPC bilayer membrane formed self-organizingly on the SiO_2 surface with small and sparse OTS islands, while did not when the OTS islands were larger and denser. The relative size between the vesicles and the SiO_2 regions is the critical factor for the formation of the DPPC bilayer membrane.

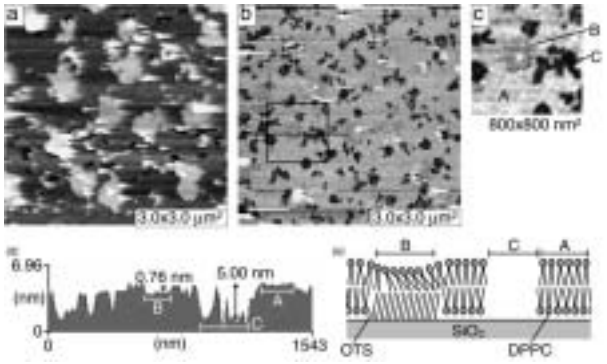

Figure 1. AFM images (3.0 × 3.0 μm^2) of the OTS-modified SiO_2 surface (θ_{OTS} = 0.21) obtained in the buffer solution (a) before and (b) after the deposition of DPPC. (c) The magnified image of the square area in (b) (800 × 800 nm^2). (d) The profile of the line drawn in (b). (e) Schematic illustration for the line profile in (d).

VI-F-2 Deposition of 10-Undecenoic Acid Self-Assembled Layers on H-Si(111) Surfaces Studied with AFM and FT-IR

LI, Yanjun; TERO, Ryugo; NAGASAWA, Takayuki; NAGATA, Toshi; URISU, Tsuneo

[*Appl. Surf. Sci.* in press]

Self-assembling layers of 10-undecenoic acid (UA) were deposited on H-terminated Si(111) surfaces and characterized with atomic force microscopy (AFM) and Fourier-transform infrared (FT-IR) spectroscopy measurements for the first time. The unique island structures are deposited by layer-by-layer growth mechanism. The IR spectra suggest that the multilayers grown over the first monolayer are deposited by weak intermolecular interactions such as Van der Waals force and hydrogen bonding.

VI-F-3 Structure and Deposition Mechanism of 10-Undecenoic Acid Self-Assembled Layers on H-Si(111) Surfaces Studied by Atomic Force Microscopy and Fourier-Transform Infrared Spectroscopy

LI, Yanjun; TERO, Ryugo; NAGASAWA, Takayuki; NAGATA, Toshi; HARUYAMA, Yuichi[1]; URISU, Tsuneo
([1]Univ. Hyogo)

[*Jpn. J. Appl. Phys.* **43**, 4591–4594 (2004)]

Ten-undecenoic acid self-assembled multilayers were deposited on H-Si(111) surfaces and the surface morphology was investigated by atomic force microscopy (AFM). Namely, we studied the H-Si(111) surface modification of –COOH terminal functional groups. Characteristic islands of almost the same height are observed. From AFM images and transmission IR spectra, it was confirmed that multilayer deposition easily occurs through weak intermolecular interactions such as the Van der Waals force and hydrogen bond interactions. The growth mechanism and film structure were discussed.

VI-F-4 Deposition of DPPC Monolayers by the Langmuir-Blodgett Method on SiO_2 Surfaces Covered by Octadecyltrichlorosilane Self-Assembled Monolayer Islands

TAKIZAWA, Morio; KIM, Yong-Hoon; URISU, Tsuneo

[*Chem. Phys. Lett.* **385**, 220–224 (2004)]

The morphology of self-assembled monolayer (SAM) islands of *n*-octadecyltrichlorosilane (OTS) deposited on chemically and thermally oxidized SiO_2 surfaces was studied by dynamic force microscopy (DFM). The shape and size of the islands were found to depend significantly on the hydrophilicity of the SiO_2 surface. Langmuir-Blodgett (LB) monolayers of a lipid, dipalmitoylphosphatidylcholine (DPPC), deposited on these SiO_2 surfaces covered by OTS-SAM islands have

shown that the DPPC monolayer is supported firmly on the SiO_2 surface by the hydrophobic islands acting as anchor molecules.

VI-F-5 Characterization of Dipalmitoylphosphatidylcholine/Cholesterol Langmuir-Blodgett Monolayers Investigated by Atomic Force Microscopy and Fourier Transform Infrared Spectroscopy

KIM, Yong-Hoon; TERO, Ryugo; TAKIZAWA, Morio; URISU, Tsuneo

[*Jpn. J. Appl. Phys.* **43**, 3860–3864 (2004)]

The addition effects of cholesterol on the dipalmitoylphosphatidylcholine (DPPC) Langmuir-Blodgett (LB) monolayer have been investigated by atomic force microscopy (AFM) and infrared reflection absorption spectroscopy (IRRAS). The phase transformation from pure DPPC to the DPPC/cholesterol phase proceeds through two stages: initial drastic changes in the surface morphology and the conformation of the DPPC acyl chains below 10% cholesterol, and the gradual homogenization of the morphology towards the liquid-order phase up to 35% cholesterol. The IRRAS peak position indicates that the conformational disorder of the acyl chain becomes almost that of the liquid level at 10% cholesterol addition. In the homogeneous liquid-order phase at 35% cholesterol, the terminal methyl groups of the DPPC are aligned in good order similarly to the solidlike gel phase, whereas the acyl chains have a liquid-level disordered conformation.

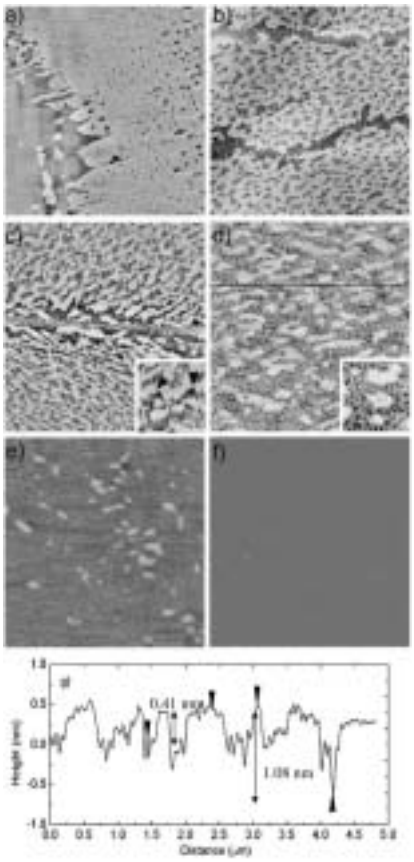

Figure 1. AFM images (5.0 × 5.0 μm^2) of DPPC/cholesterol LB monolayers transferred onto the mica surface at the surface pressure of 10 mNm^{-1}. The concentrations of cholesterol are a) 0% (pure DPPC), b) 5%, c) 10%, d) 20%, e) 30% and f) 35% in molar ratio. g) The profile of the line drawn in d). The scale of the insets in (c) and (d) is 1.34 × 1.34 μm^2.

VI-F-6 An AFM Characterization of Gramicidin A in Tethered Lipid Membrane on Silicon Surface

LEI, Shenbin; TERO, Ryugo; MISAWA, Nobuo; WAN, Lijun; URISU, Tsuneo

Recently there has been growing interest in supported bilayer lipid membranes (sBLMs). The supported lipid membrane is much more stable in comparison with the unsupported lipid membrane, extending their life from hours to a period of days withstanding mechanical distortion and repeated washes. This stability of sBLMs enables its research applications such as use in developing biosensors and surface coatings.[1)]

Here we use the avidin-biotin interaction, which is known to be one of the strongest bindings between a protein and a ligand and is a key example of the biological specificity and the biological adaptation,[2)] to form a tethered phospholipid membrane on oxidized Si(100) surfaces. The procedure for our strategy is schematically shown in Scheme 1. AFM characterizations show avidin molecules are well dispersed and the surface density is estimated to be about 40 molecule/μm^2. When sonicated unilamellae vesicles (SUVs) (0.3 mM DPPC in 0.1 M HEPES buffer) containing 2% mol gramicidin A was deposited on this surface, single lipid bilayers formed in the large area, but with high density of defects as compared with that on the mica surface. The thickness of this bilayer is measured to be 5.8 to 6.1 nm, in consistent with previous reports. In the tethered membrane, gramicidin A appear as depressions, which is the same as reported for gramicidin in supported membrane on mica. However, the topography is significantly different. On mica surface, gramicidin A aggregates into linear structures. However, in the tethered membrane on the silicon surface, both linear and spot like gramicidin aggregations appear. The width and height of these depressions are also different in the tethered membrane as compared with that in the supported membrane on mica. Also, in the tethered membrane, gramicidin appears with higher density than expected. These results seem to indicate that gramicidin A aggregates into larger aggregations in the supported membrane than in the tethered membrane. Certainly the current conclusion needs further characterizations to make it more solid.

References

1) U. Rädler, J. Mack, N. Persike, G. Jung and R. Tampé, *Biophys. J.* **79**, 3144 (2000).
2) A. Torreggiani, G. Bottura and G. Fini, J. Raman *Spectrosc.* **31**, 445 (2000).

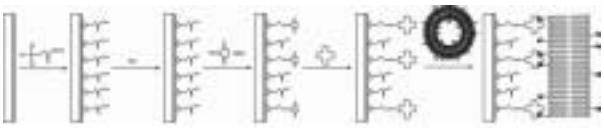

Figure 1. Scheme 1.

VI-F-7 Immobilization of Avidin on COOH-Modified SiO_2/Si(100) Surface and Characterization by AFM and BML-IRRAS

MISAWA, Nobuo; YAMAMURA, Shusaku; URISU, Tsuneo

Nowadays bio-mimetic sensing techniques, using immobilization of intact biomolecules on solid surfaces, attract significant attentions. For solid substrates, silicon is a suitable material since precise micro-fabrication has been established. New biosensors can be combined with electronics devices on the same chip. Characterizations by IR spectroscopy and AFM observation are useful tools to investigate biomolecules immobilized on silicon surface. It is known that BML-IRRAS (Infrared Reflection Absorption Spectroscopy using Buried Metal Layer substrate[1)]) is a high-resolution surface vibration spectroscopy on the semiconductor or insulator materials, which has sub-monolayer sensitivity for the wide frequency range including fingerprint regions. In this study we have immobilized avidin, which has high versatility for conjugation of biomolecules with solid surfaces, on the SiO_2/Si(100) surface modified with carboxyl groups, and characterized the surface by AFM and BML-IRRAS for the first time. The –COOH modification was produced by the deposition of 2-(carbomethoxy)ethyltrichlorosilane and sequential hydrolysis by HCl. Immobilization of avidin was performed after condensation reaction by N-hydroxysucciniimide and EDC, which enhanced the reactivity of carboxyl group with amino group of avidin.

AFM images (Figure 1) showed that the roughness of the –COOH modified surface was less than 0.5 nm, and protrusions with about 15 nm diameter and 2 nm height appeared after the avidin immobilization. The BML-IRRAS measurements showed clear peaks at 1650 cm^{-1} and 1550 cm^{-1}, which were assigned to Amide I and Amide II bands of avidin. These bands also consisted of several fine structures which might be assigned to secondary structures such as α-helix and β-sheet *etc.* The detailed shape analysis of these bands could give the information with orientations of these immobilized proteins.

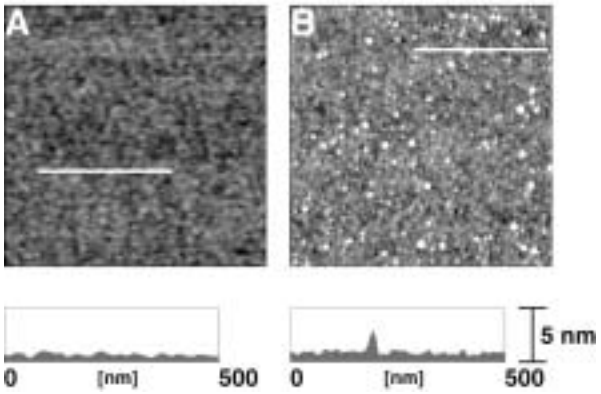

Figure 1. AFM images (1.0 μm × 1.0 μm) and line profiles of COOH-modified surfaces (A) before and (B) after immobilization of avidin.

Reference

1) S. Yamamura. *et al.*, *Jpn. J. Appl. Phys.* **42**, 3942 (2003).

VI-G Photoionization and Photodissociation Dynamics Studied by Electron and Fluorescence Spectroscopy

Molecular photoionization is a major phenomenon in vacuum UV excitation and provides a large amount of information on fundamental electron-core interactions in molecules. Especially, neutral resonance states become of main interest, since they often dominate photoabsorption cross sections and lead to various vibronic states which are inaccessible in direct ionization. We have developed a versatile machine for two-dimensional photoelectron spectroscopy in order to elucidate dynamical aspects of superexcited states such as autoionization, resonance Auger decay, predissociation, vibronic couplings, and internal conversion. In a two-dimensional photoelectron spectrum (2D-PES), the photoelectron yield is measured as a function of both photon energy $E_{h\nu}$ and electron kinetic energy E_k (binding energy). The spectrum, usually represented as a contour plot, contains rich information on photoionization dynamics.

Photofragmentation into ionic and/or neutral species is also one of the most important phenomena in the vacuum UV excitation. In some cases, the fragments possess sufficient internal energy to de-excite radiatively by emitting UV or visible fluorescence. It is widely accepted that fluorescence spectroscopy is an important tool to determine the fragments and to clarify the mechanisms governing the dissociation processes of diatomic and polyatomic molecules. For several years we have concentrated our energies on fluorescence spectroscopy of H_2O in the photon energy region of 15–55 eV.

VI-G-1 Photofragmentaion Mechanisms of H_2O Studied by Ultraviolet Dispersed Spectroscopy

MITSUKE, Koichiro

[*J. Electron Spectrosc. Relat. Phenom.* submitted]

Fragmentation of H_2O has been studied by dispersed fluorescence spectroscopy at excitation photon energies above 20 eV. Figure 1 shows expanded dispersed spectra in the wavelength range from 280 to 420 nm. With appearance energies of $h\nu \sim 30$ eV several vibrational bands, marked with diamond symbols, begin to emerge below 320 nm. We have assigned these peaks to OH($A^2\Sigma^+ \rightarrow X\ ^2\Pi$) transition, judging from characteristic peaks due to the R_1 band heads for the $\Delta v = v' - v'' = 0$ sequence at 306.4, 312.6, and 318.8 nm. The counter fragment of OH($A^2\Sigma^+$) must be H*(n) in the Rydberg state with $n \geq 2$. The above appearance energies are much higher than the dissociation limits for the OH ($A^2\Sigma^+$) + H*($n \geq 2$) channels, but in good agreement with the vertical transition energies[2] for the associated Rydberg states of H_2O.

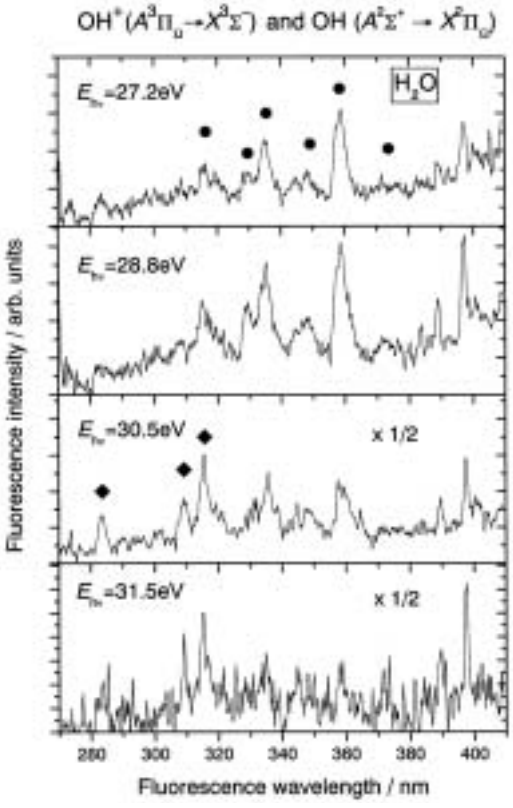

Figure 1. Dispersed fluorescence spectra of H_2O. The symbols ● and ◆ designate the vibrational bands due to the $OH^+(A^3\Pi \rightarrow X\ ^3\Sigma^-)$ and OH($A\ ^2\Sigma^+ \rightarrow X\ ^2\Pi$) transitions, respectively.

References

1) K. Mitsuke, *J. Chem. Phys.* **117**, 8334–8340 (2002).
2) J. Appell and J. Durup, *Int. J. Mass Spectrom. Ion Phys.* **10**, 247–265 (1972/73).

VI-G-2 Autoionization and Neutral Dissociation of Superexcited HI Studied by Two-Dimensional Photoelectron Spectroscopy

HIKOSAKA, Yasumasa; MITSUKE, Koichiro

[*J. Chem. Phys.* **121**, 792–799 (2004)]

Two-dimensional photoelectron spectroscopy of

hydrogen iodide HI has been performed in the photon energy region of 11.10–14.85 eV, in order to investigate dynamical properties on autoionization and neutral dissociation of Rydberg states HI*(R_A) converging to $HI^+(\tilde{A}\,^2\Sigma^+_{1/2})$. A two-dimensional photoelectron spectrum exhibits strong vibrational excitation of $HI^+(\tilde{X}^2\Pi)$ over a photon energy region from ~ 12 to 13.7 eV, which is attributable to autoionizing feature of the 5$d\pi$ HI*(R_A) state. A noticeable set of stripes in the photon energy region of 13.5–14.5 eV are assigned as resulting from autoionization of the atomic Rydberg states of I* converging to $I^+(^3P_0$ or $^3P_1)$. The formation of I* is understood in terms of predissociation of multiple HI*(R_A) states by way of the repulsive Rydberg potential curves converging to $HI^+(^4\Pi_{1/2})$.

VI-H Development of the Laser-SR Combination System for Photodissociation Studies of Highly Vibrationally Excited Molecules

Initial vibrational excitation in molecules might influence the chemical branching in photodissociation, if two or more different dissociation pathways are accessible from an electronically excited state. Much attention has been focused on the pioneering work of Crim and his collaborators [*J. Chem. Phys.* **92**, 803–805 (1990)], who could accomplish the selective bond-breaking of heavy water, HOD. Very recently Yokoyama, Akagi and coworkers reported that deuterized ammonia NHD_2 in the fourth N–H stretching overtone preferentially photodissociates into the ND_2 + H channel [*J. Chem. Phys.* **118**, 3600–3611 (2003)]. In these two studies UV lasers are employed for vibrationally mediated photodissociation.

Instead, we are planning to use synchrotron radiation (SR) to promote vibrationally excited molecules to electronically excited states in the vacuum UV region. The main objectives are as follows: (1) Elucidating the properties of dissociative states by sampling a wide range of their potential energy surfaces, such as dynamics determining the final-state distributions of the products, nonadiabatic transitions on dissociation, and assignments and characterization of unknown multiply-excited states produced by Auger decay from core-excited states. (2) Aiming at more universal "vibrational state-specific" rupture of chemical bonds, which could be realized by changing the overlap between the wavefucntions of the upper-state continuum and that of the ground state.

VI-H-1 Apparatus for Probing Dissociative Photoionization of Vibrationally Excited H_2O into $OH^+(X^3\Sigma^-)$ + H(n = 1)

MITSUKE, Koichiro; MORI, Takanori; KOU, Junkei; ADACHI, Junichi[1]; YAGISHITA, Akira[1]; AKAGI, Hiroshi[2]; YOYAMA, Atsushi[2]
([1]KEK-PF; [2]JAERI, Tokai)

We have developed an experimental system for laser-SR two photon ionization the crux of which are an ultrahigh resolution continuous titanium-sapphire laser (a bandwidth of 4×10^{-4} cm^{-1}) and in-vacuum beam alignment devices for strict overlapping of the counter-propagating two photon beams. The apparatus was connected to the beam line 28A of the Photon Factory synchrotron radiation facility in Tsukuba. Figure 1 shows a schematic diagram of the experimental setup. The wavenumber of the laser was determined precisely in the range of from 13814 to 13819 cm^{-1} by observing photoacoustic signal from laser excited H_2O measured with a lock-in modulation technique. The photon beam alignment devices are situated upstream and downstream of a central photoionization chamber. Each device is comprised of two stainless steel plates fitted on two-dimensional motion feedthroughs individually adjustable: one plate has an aperture of 0.8 mmϕ and the other plate is coated with a fluorescing substance. These plates can be inserted across the photon beam axis without breaking the system vacuum, which permits us to easily attain good spatial overlap of the two beams. The OH^+ ions produced via dissociation of $H_2O^*(4\nu_{O-H}) + h\nu \rightarrow OH^+(X^3\Sigma^-) + H(n = 1) + e^-$ were detected by time-of-flight mass spectrometry at SR photon energies near the dissociation threshold of 18.05 eV with respect to the neutral ground state of water.

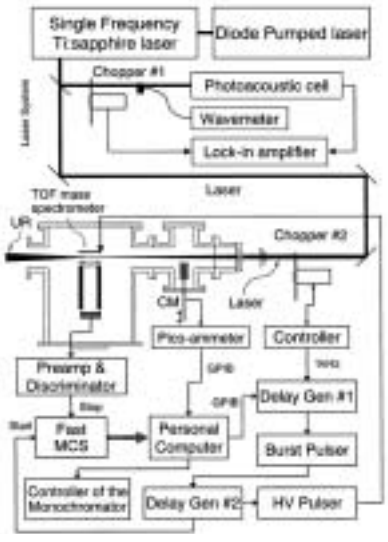

Figure 1. Schematic diagram of the setup for laser-SR two photon ionization experiments.

VI-I Extreme UV Photoionization Studies of Polyatomic Molecules and Fullerenes by Employing a Grazing-Incidence Monochromator

On the beam line BL2B2 in UVSOR a grazing incidence monochromator has been constructed which supplies photons in the energy region from 20 to 200 eV [M. Ono, H. Yoshida, H. Hattori and K. Mitsuke, *Nucl. Instrum. Methods Phys. Res., Sect. A* **467-468**, 577–580 (2001)]. This monochromator has bridged the energy gap between the beam lines BL3B and BL4B, thus providing for an accelerating demand for the high-resolution and high-flux photon beam from the research fields of photoexcitation of inner-valence electrons, *L*-shell electrons in the third-row atom, and 4*d* electrons of the lanthanides. Since 2001 we have measured photoion yield curves of fullerenes. Geometrical structures and electronic properties of fullerenes have attracted widespread attention because of their novel structures, novel reactivity, and novel catalytic behaviors as typical nanometer-size materials. Moreover, it has been emphasized that the potential for the development of fullerenes to superconductors ($T_c \sim 50$ K) and strong ferromagnetic substances is extremely high. In spite of such important species spectroscopic information is very limited in the extreme UV region, which has been probably due to difficulties in obtaining enough number density of the sample. The situation has been rapidly changed in these few years, since the techniques of syntheses, isolation, and purification have been advanced so rapidly that appreciable amount of fullerenes is obtainable from several distributors in Japan.

VI-I-1 Kinetic Energy Distribution and Anisotropy of Fragment Ions from SF_6 by Photoexcitation of a Sulfur 2p-Electron

ONO, Masaki[1]; MITSUKE, Koichiro
([1]Chiba Univ.)

[*Chem. Phys. Lett.* **379**, 248–254 (2003)]

The kinetic energy (KE) distribution and asymmetry parameter β have been studied for photofragmentation of SF_6 near the sulfur 2*p* ionization edges at 170–208 eV by using synchrotron radiation. The relative yield of fast ions with KE > 5 eV is larger in the post-edge than in the pre-edge region, whereas β of such ions is lower in the post-edge region. The β curve shows a sudden drop from 0.06–0.07 to zero near the edges and remains constant thereafter. These results are ascribed to *LVV* Auger decay occurring above the edges leading to SF_6^{2+} and SF_6^{3+} transiently. At KE > 2 eV the distribution curve for core excitation to the $(2t_{1u})^{-1}(6a_{1g})^1$ state resembles that for valence-electron ionization at 170 eV. This agreement, together with a similarity in β, suggests that the S 2p → $6a_{1g}$ resonance transition and valence-electron ionization undergo similar formation pathways leading to fast F^+ ions (*i.e.* participation of shake-up satellite states).

VI-I-2 Production of Doubly Charged Ions in Valence Photoionization of C_{60} and C_{70} at $h\nu$ = 25–150 eV

KOU, Junkei; MORI, Takanori; S. V. K. Kumar[1]; HARUYAMA, Yusuke[2]; KUBOZONO, Yoshihiro[3]; MITSUKE, Koichiro
([1]IMS and Tata Inst. Fund. Res.; [2]Okayama Univ.; [3]IMS and Okayama Univ.)

[*J. Chem. Phys.* **120**, 6005–6009 (2004)]

Photoion yields from gaseous fullerenes, C_{60} and C_{70}, for production of singly and doubly charged ions are measured by mass spectrometry combined with tunable synchrotron radiation at $h\nu$ = 25–150 eV. Since the signal of triply or highly charged ions is very weak, the total photoionization yield curve can be estimated from the sum of the yields of the singly and doubly charged ions. There is distinct disagreement between the resultant curve of C_{60} and the calculated total photoabsorption cross section previously reported. This difference is understood by the assumption that C_{60}^{2+} ions are chiefly produced by spectator Auger ionization of the shape resonance states followed by tunneling of the trapped electron or by cascade Auger ionization. For C_{60} and C_{70} the ratios between the yields of doubly and singly charged ions are larger than unity at $h\nu$ > 50 eV. These ratios are quite different from those reported in the experiments using electron impact ionization.

VI-I-3 Absolute Photoabsorption Cross Section of C_{60} in the Extreme Ultraviolet

MORI, Takanori; KOU, Junkei; HARUYAMA, Yusuke[1]; KUBOZONO, Yoshihiro[1]; MITSUKE, Koichiro
([1]Okayama Univ.)

[*J. Electron Spectrosc. Relat. Phenom.* submitted]

The absolute photoabsorption cross section curve of C_{60} has been determined by means of mass spectrometry with the photon source of monochromatized synchrotron radiation of $h\nu$ = 24.5–150 eV. Experiments are carried out using a high-temperature source of gaseous fullerenes and an efficient time-of-flight mass spectrometer. The absolute cross section curve is shown in Figure 1. The cross sections are 762, 241 and 195 Mb at $h\nu$ = 24.5, 90, and 110 eV, respectively with about 10% errors. Our results may suffer from some deviation from the real cross section curve. This deviation chiefly arises from uncertainties in the number density *n* of C_{60} in the ionization region, because we derive *n* from the

mass deposition rate at the thickness monitor by assuming effusive flow conditions for the properties of the C_{60} beam. The present cross section curve was then normalized at $h\nu$ = 25 eV to the absolute cross section reported by Jaensch and Kamke,[1] the most reliable data so far available in the valence region of C_{60}. Eventually, the present cross section data were reduced to 407, 144 and 114 Mb at $h\nu$ = 25, 90, and 110 eV, respectively.

References

1) R. Jaensch and W. Kamke, *Mol. Materials* **13**, 143–150 (2000).
2) J. Berkowitz, *J. Chem. Phys.* **111**, 1446–1453 (1999).

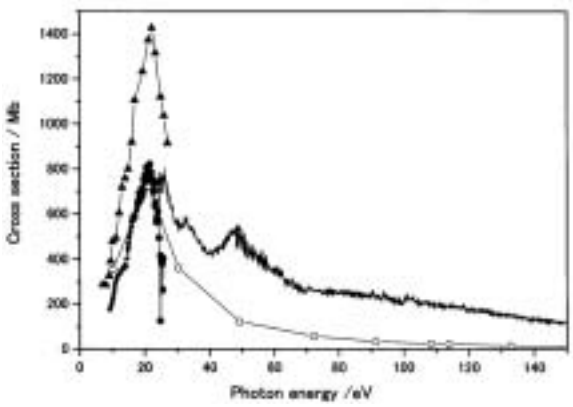

Figure 1. Absolute absorption cross section of C_{60} at $h\nu$ = 24.5–150 eV (solid line). The closed circles and triangles designate the data measured by Jaensch and Kamke[1] and those compiled by Berkowitz,[2] respectively. The open circles indicate the cross section of sixty carbon atoms.

VI-I-4 Photofragmentation of C_{60} in Valence Ionization

KOU, Junkei; MORI, Takanori; KUBOZONO, Yoshihiro[1]; MITSUKE, Koichiro
([1]Okayama Univ.)

[*J. Electron Spectrosc. Relat. Phenom.* submitted]

The yield curves for C_{60-2n}^{+} (n = 1–3) produced by photoionization of C_{60} were measured in the $h\nu$ range of 25–150 eV. The appearance energies increase with increasing n, as evidenced from Figure 1. Evaluation was made on the upper limits of the internal energies of the primary C_{60}^{+} above which $C_{60-2n+2}^{+}$ fragments ($n \geq 1$) cannot escape from further dissociating into $C_{60-2n}^{+} + C_2$. These limits agree well with the theoretical internal energies of C_{60}^{+} corresponding to the formation threshold for C_{60-2n}^{+}, assuming that the binding energies of $C_{60-2n+2}^{+}$ are equal to those proposed by Foltin *et al.*[1]

Reference

1) M. Foltin, M. Lezius, P. Scheier and T. D. Märk, *J. Chem. Phys.* **98**, 9624–9634 (1993).

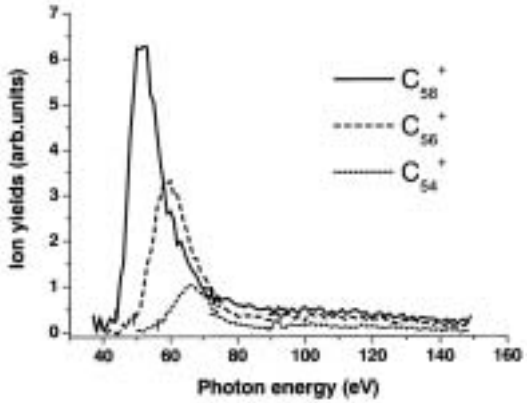

Figure 1. Yield curves for C_{60-2n}^{+} ions (n = 1–3) obtained from time-of-flight mass spectra.

VI-I-5 Remarkably Large Shifts of the Appearance Energies of C_{60-2n}^{z+} ($n \geq 1$) from Their Thermochemical Thresholds

KOU, Junkei; MORI, Takanori; KUBOZONO, Yoshihiro[1]; MITSUKE, Koichiro
([1]Okayama Univ.)

[*Phys. Chem. Chem. Phys.* submitted]

The ion yield curves for C_{60-2n}^{z+} (n = 1–5, z = 1–3) produced by photoionizaiotion of C_{60} have been measured in the $h\nu$ range of 25–150 eV. The appearance photon energies are higher by 30–33 eV than the thermochemical thresholds for dissociative ionization of C_{60} leading to $C_{60-2n}^{z+} + C_2$. With increasing n the appearance energies shift to higher $h\nu$ positions for a given z. Evaluation is made on the upper limits of the internal energies of the primary C_{60}^{z+} above which $C_{60-2n+2}^{z+}$ fragments ($n \geq 1$) cannot escape from further dissociating into $C_{60-2n}^{z+} + C_2$. These upper limits agree well with the theoretical internal energies of C_{60}^{z+} corresponding to the threshold for the formation of C_{60-2n}^{z+}. The photofragmentation of C_{60}^{z+} is considered to be governed by the mechanism of internal conversion of the electronically excited states of C_{60}^{z+}, statistical redistribution of the excess energy among a number of vibrational modes, and successive ejection of the C_2 units.

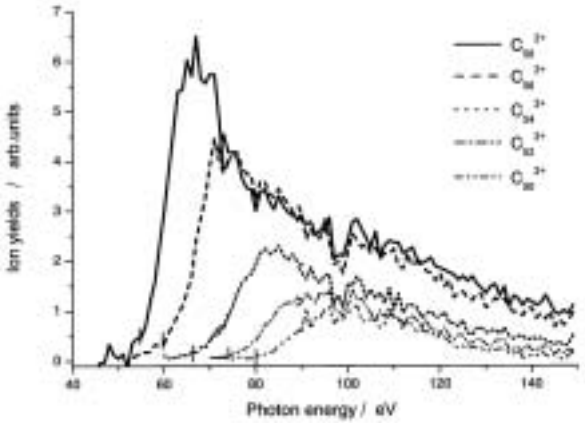

Figure 1. Yield curves of C_{60-2n}^{2+} ions (n = 1–5) obtained from time-of-flight mass spectra.

VI-I-6 Photoion Yields from Ce@C_{82} near the 4*d* Edge of Ce

MITSUKE, Koichiro; MORI, Takanori; KOU, Junkei; HARUYAMA, Yusuke[1]; KUBOZONO, Yoshihiro[1]
([1]Okayama Univ.)

The yield curves for photoions from Ce@C_{82} are measured by using synchrotron radiation in the photon energy range from 90 to 160 eV. Parent Ce@C_{82}^{z+} and fragment ions C_{60}^{z+} and C_{70}^{z+} are observed in a mass spectrum (z = 1 and 2). The yield curves for principal ionic species exhibit broad resonance in the region $h\nu$ =120–140 eV which is ascribed to the $4d \rightarrow \varepsilon f$ giant dipole resonance of the encapsulated Ce atom. The total photoabsotpion cross section of Ce@C_{82} was determined from partial photofragmentation cross sections for respective ions to be $19.6^{+6.5}_{-3.9}$ and $5.3^{+1.8}_{-1.1}$ Mb at $h\nu$ = 110 and 130 eV, respectively.

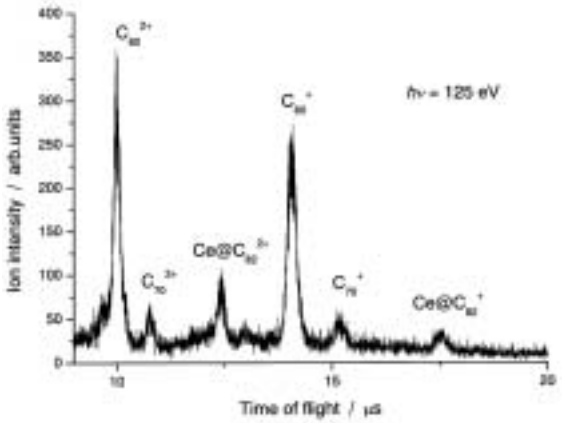

Figure 1. Time-of-flight mass spectrum of the parent and fragment ions produced by photoionization of Ce@C_{82} at $h\nu$ = 125 eV.